The SAM Model for Wear Inhibitor Performance of Dithiophosphates on Iron Oxide

Shaoyi Jiang,[†] Rawls Frazier,[‡] Elaine S. Yamaguchi,[§] Mario Blanco,[†] Siddharth Dasgupta,[†] Yanhua Zhou,[†] Tahir Cagin,[†] Yongchun Tang,[||] and William A. Goddard, III*,[†]

Materials and Process Simulation Center, Beckman Institute (139-74), Division of Chemistry and Chemical Engineering, California Institute of Technology, Pasadena, California 91125, Chevron Research and Technology Company, 100 Chevron Way, Richmond, California 94802, Chevron Chemical Company, Oronite Technology Group, 100 Chevron Way, Richmond, California 94802, and Chevron Petroleum Technology Company, 1300 Beach Boulevard, La Habra, California 90631

Received: November 18, 1996; In Final Form: March 12, 1997[⊗]

Zinc dithiophosphate (DTP) molecules have long been used as wear inhibitor oil additives for automotive engines. In order to obtain an atomistic understanding of the mechanism by which these molecules inhibit wear, we examined the geometries, energetics, and vibrations of an oxidized iron surface [(001) surface of α-Fe_2O_3] using the MSX force field (FF) based on *ab initio* quantum chemistry (QC) calculations. The DTP molecules studied include $(RO)_2PS_2$ with R = methyl, isobutyl, isopropyl, and phenyl. The α-Fe_2O_3 surface is described using the generalized valence bond (GVB) model of bonding. The geometries, binding energies, and vibrational frequencies from *ab initio* calculations on simple clusters are used with the biased Hessian method to develop the MSX FF suitable for describing the binding of DTP molecules to the surfaces. We find that the cohesive energies for the self-assembled monolayers (SAM) of the DTP molecules on the Fe_2O_3 surface correlate with the antiwear performance observed in experimental engine tests. This suggests that the search for more effective and environmentally benign wear inhibitors can use the cohesive energies for SAM formation as a criterion in selecting and prioritizing compounds for experimental testing.

I. Introduction

Zinc dithiophosphates [$Zn(DTP)_2$, where DTP = $(RO)_2PS_2$] have been used extensively as antiwear agents for about 40 years. The structure for the monomer is shown in Figure 1. [In various nonpolar solvents (e.g., hexane) $Zn(DTP)_2$ forms an equilibrium involving substantial amounts of dimer, trimer, etc.[1]] The antiwear mechanism for these remarkable materials is not understood.[2,3] This was previously of little concern since they are cheap and effective. However, industrial priorities (ILSAC, GF-2) and environmental concerns[4] make it necessary to find replacements for $Zn(DTP)_2$ that are equally efficient yet environmentally benign antiwear additives for lubricant oils. No reliable procedures have been developed for assessing the wear performance (in order to prioritize experiments) except direct engine testing, which is slow and enormously costly.[5] Interaction of the DTP molecules with the iron and iron oxide surface in the engine is expected to be important for lubrication and wear properties. There have been experimental studies of the performance of various DTPs on engine surfaces.[6] However, film formation on these surfaces is not understood at the molecular level.

In order to help provide better evidence in selecting and prioritizing new candidates for wear inhibitors, we initiated a program to use atomistic simulation techniques to study the mechanism of wear inhibition. Our goal is to (a) develop theoretical principles for understanding the antiwear mechanism afforded by the oil additives, (b) use these principles to suggest new structures of useful oil additives and to order the priorities for subsequent tests, and (c) improve the reliability of bench wear tests for evaluating the effectiveness of potential engine oil additives.

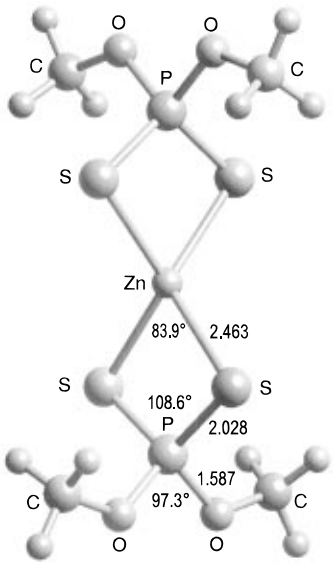

Figure 1. Structure of the $Zn(DTP)_2$ monomer from QC calculations (HF/LAV3P***). Here R = CH_3 and the net charge is zero.

Previously,[7] we reported structural and vibrational analyses of ZnDTP molecules from *ab initio* quantum chemistry (QC). These results[7] showed that the two P−S bonds of the dithiophosphate of ZnDTPs are *equivalent*, with a bond order of $1^1/_2$. This leads to a strong *antisymmetric P−S stretch* IR transition at about 650 cm^{-1} and a weaker *symmetric P−S stretch* transition at about 540 cm^{-1}. We developed[7] the MSX force field (FF) based on the QC and studied geometries, binding energies, and vibrations of DTP with R = methyl (Me), isobutyl (iBu), isopropyl (iPr), and phenyl (Ph).

We assume that the iron surface in the engine is oxidized, and hence we examine chemisorption of DTP on the (001)

* To whom correspondence should be addressed.
[†] California Institute of Technology.
[‡] Chevron Research and Technology Co.
[§] Chevron Chemical Co.
[||] Chevron Petroleum Technology Co.
[⊗] Abstract published in *Advance ACS Abstracts,* September 1, 1997.

S1089-5647(96)03835-7 CCC: $14.00

surface of α-Fe_2O_3. We find that each DTP can form a stable self-assembled monolayer (SAM) on a Fe_2O_3 surface and that the cohesive energy of the SAM correlates well with experimental engine wear performance measurements. This correlation has allowed us to use modeling strategies to evaluate the likely performance of new environmentally benign additives [e.g., ashless (no metal) wear inhibitors] prior to experiment.[8]

This approach of developing a simple model for the structure and energies of SAMs in order to provide a basis for comparing their effectiveness as inhibitors may also be useful in other applications involving the interaction of molecular species with metals and metal oxide surfaces.[9]

Section II describes calculational details for the *ab initio* QC and FF methods used here. Section III develops the FF for DTP on Fe_2O_3. Section IV reports the geometries, energetics, and vibrations for various DTPs on cluster and surface. The results are summarized in section V, and the conclusion is in section VI.

II. Calculational Details

II.A. Quantum Chemistry. Unless stated otherwise, all QC calculations were carried out with the PS-GVB program[10,11] at the Hartree−Fock (HF) level using the LAV3P*** basis set. The LAV3P basis set[11,12] describes the atoms Na−La and Hf−Bi with the Hay and Wadt valence-only effective core potentials (ECP)[12] and the atoms H−Ne with the all-electron 6-31G basis.[13] This basis set differs from LAN1DZ[12] in that the three s basis functions are left uncontracted (the rest of the basis uses the standard double-ζ contraction). The notation *** indicates that d polarization functions (exponent = 0.074) are added for Fe, d polarization functions (exponent = 0.80, 0.80, 0.3934, 0.487) are added for (C, O, P, S, respectively), and p polarization functions (exponent = 1.10) are added for H. It was found[7] that the LAV3P*** basis and ECP produces results in good agreement with all-electron calculations.

Molecular charges are based on the electrostatic field[14] from *ab initio* HF calculations. In this procedure, the electrostatic field is calculated over a grid of points from the HF wave function. Using the grid points outside of the van der Waals (vdw) radii, atom-centered charges are derived to match the HF potential while reproducing the dipole moment from HF.

II.B. The MSX Force Field and Charges. The universal force field (UFF)[15b] was modified to fit the *ab initio* calculations using biased Hessian techniques.[16] The FF describes the total potential energy of a molecule as a superposition of short-range valence terms (E_{val}) plus long-range nonbonded (E_{nb}) interactions,

$$E = E_{val} + E_{nb} \tag{1}$$

The valence interactions consist of bond stretch (E_{bond}), bond-angle bend (E_{angle}), dihedral angle torsion ($E_{torsion}$), and inversion ($E_{inversion}$) terms,

$$E_{val} = E_{bond} + E_{angle} + E_{torsion} + E_{inversion} \tag{2}$$

For E_{bond} we use either harmonic terms

$$E^{H}_{bond} = \frac{1}{2}K_R(R - R_0)^2 \tag{3a}$$

or Morse

$$E^{M}_{bond} = D_R[e^{-\alpha(R-R_0)} - 1]^2 \tag{3b}$$

where $\alpha = \sqrt{K_R/2D_R}$. For angle terms we use the dihedral cosine harmonic terms[15]

$$E_{angle} = \frac{1}{2}\frac{K_\theta}{(\sin\theta_0)^2}(\cos\theta - \cos\theta_0)^2 \tag{4a}$$

and in some cases we include angle−stretch and stretch−stretch coupling,

$$E_x = K_{R_1\theta}(R_1 - R_{10})(\theta - \theta_0) + K_{R_2\theta}(R_2 - R_{20})(\theta - \theta_0) + K_{RR}(R_1 - R_{10})(R_2 - R_{20}) \tag{4b}$$

For $E_{torsion}$ we use

$$E_{torsion} = \frac{1}{2}V_3(1 + \cos 3\phi) \tag{5}$$

The nonbonded interactions consist of vdw (E_{vdw}) and electrostatic (E_Q) terms,

$$E_{nb} = E_{vdw} + E_Q \tag{6}$$

For E_{vdw} we use[15] exponential-6

$$E^{x6}_{vdw} = D_v\left\{\left[\left(\frac{6}{\zeta-6}\right)\exp^{\zeta(1-R/R_v)}\right] - \left[\left(\frac{\zeta}{\zeta-6}\right)\left(\frac{R}{R_v}\right)^6\right]\right\} \tag{7}$$

or Morse

$$E^{M}_{vdw} = D_v[\chi^2 - 2\chi] \tag{8a}$$

where

$$\chi = \exp\left[-\frac{\zeta}{2}\left(\frac{R}{R_v} - 1\right)\right] \tag{8b}$$

For E_Q we use

$$E_Q = \sum_{i>j}\frac{Q_iQ_j}{\epsilon_0 R_{ij}} \tag{9}$$

(where $1/\epsilon_0$) = 332.0637 if E is in kcal/mol, R is in Å, and charges are in electron units).

The equilibrium bond lengths (R_0) and angles (θ_0) were fitted to the *ab initio* geometries. The force constants (K_b, K_θ, $K_{R\theta}$, and K_{RR}) were fitted to the *ab initio* vibrational frequencies using the biased Hessian method.[16,17] The torsional barriers (V_m) were adjusted to reproduce the conformational energy differences from the HF calculations. Nonbonded interactions (vdw and Q) are not used between nearest neighbors (1−2 interactions) and next-nearest neighbors (1−3 interactions). The dielectric constant is taken as $\epsilon = 1$.

The purpose of developing the MSX FF is to predict accurate structural, vibrational, and energetic properties of large molecules. Thus it is essential to have a general approach for predicting the charges for large systems. We used the charge equilibration (QEq) method[18,19] but with the parameters readjusted to reproduce the *ab initio* charges from quantum calculations on model systems. This is denoted as QEq*.

For metal−DTP systems the Fe−S interactions was treated as a nonbonded interaction just as for the Zn−S interactions of ZnDTP systems.[7] That is, they were described with vdw and electrostatic terms [(7)−(9)] but without valence terms [(3)−(5)]. This allows DTP to dissociate smoothly from the metal surfaces.

For bulk and surface Fe_2O_3 and for OH_2 and OH interacting with Fe, we used Morse functions adjusted to fit the QC of $Fe(OH)_3(H_2O)_3$ clusters and the structure of bulk Fe_2O_3. As

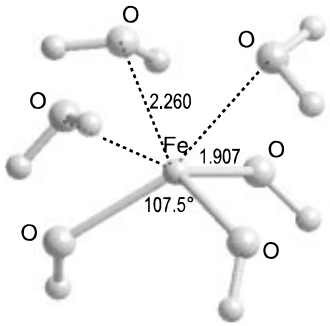

Figure 2. *Ab initio* geometries from QC calculations (HF/LAV3P***) of the GVB cluster model for the octahedral site in α-Fe_2O_3.

described below, the GVB model of the oxides suggests that there are three CPI bonds for which we use the Morse bond (3b) interaction and three DA bonds for which we use the Morse nonbonded (8) term. This allows H_2O to dissociate smoothly from the metal surface.

The FF parameters were adjusted to fit *ab initio* geometry, bond energy, and vibrational frequency from HF calculations on clusters containing DTP bonded to the metal. This FF is denoted as MSX (materials simulation with limited cross terms).

II.C. Vibrations. Vibrational frequencies were obtained by diagonalizing the full second-derivative matrix (Hessian) evaluated at the optimum HF structure using HF/LAV3P***. The infrared intensities were also computed from coupled perturbed Hartree−Fock (CPHF) calculations of the derivative of the dipole moment with respect to changes in the nuclear coordinates.

III. The FF for DTP on Fe_2O_3

III.A. The Generalized Valence Bond Model of α-Fe_2O_3. Depending on environmental conditions, the surface of iron may involve various forms of iron oxide. We consider here that it is hematite or α-Fe_2O_3.[20] In order to develop a FF for Fe_2O_3, we use the generalized valence bond (GVB) concept,[9,21] which assumes that Fe^{3+} makes three covalent, partially ionic (CPI) bonds (corresponding to the formal charge of +3), with the remaining three bonds being of donor−acceptor (DA) or Lewis base−Lewis acid type [involving a lone pair of electrons on the O (the Lewis base) coordinating to an empty orbital on the Fe (the Lewis acid)]. Indeed, in α-Fe_2O_3 the Fe is in a distorted octahedral site with three bonds at 1.946 Å (with OFeO bond angles of 102.5°) and three at 2.116 Å. Thus, we interpret the three 1.946 Å bonds as CPI and the three 2.116 Å bonds as DA.

To test this GVB model we carried out quantum mechanical calculations (HF/LAV3P***) on the $Fe(OH)_3(H_2O)_3$ complex. We find the structure in Figure 2 with three CPI bonds of 1.907 Å (with OFeO bond angles of 107.5°) and three DA bonds of 2.260 Å. All vibrational frequencies are positive, showing that the structure is stable. The other key quantities are tabulated in Table 1. The close correspondence of the geometries for the $Fe(OH)_3(H_2O)_3$ cluster and the Fe_2O_3 crystal confirms the GVB model of Fe_2O_3. In this model the CPI bond is expected to be approximately trans to a DA bond, and indeed, the cluster leads to an average angle of 159.7°, while the crystal leads to 162.2°.

Based on the *ab initio* calculations, we developed the MSX FF for the $Fe(OH)_3(H_2O)_3$ cluster. This FF reproduces the *ab initio* geometries of the cluster, the snap bond energy[22] (23.8 kcal/mol) for H_2O in the cluster, and the snap bond energy[23] (134.5 kcal/mol) for OH in the cluster. The charges are obtained using QEq* where the parameters[18] were modified to fit the QC (Tables 2 and 3). Table 1 shows that the geometries from the MSX FF are in excellent agreement with HF results.

TABLE 1: Comparison of *ab Initio* and FF Geometries[a] for the $Fe(OH)_3(H_2O)_3$ Cluster; The Overall Symmetry is C_3

type	no.	QC[b]	MSX	UFF	Fe_2O_3 crystal
O−H	9	0.946	0.946	0.995	
Fe−O	3	1.907	1.906	1.904	1.946
Fe...O	3	2.260	2.257	2.364	2.116
H−O−H	3	108.2	108.2	104.2	
O−Fe−O	3	107.5	107.4	87.5	102.5
Fe−O−H	3	121.3	121.2	102.7	
O···Fe−O	3	159.7	160.7	166.5	162.2

[a] Bond lengths are in angstroms, and bond angles are in degrees. [b] HF/LAV3P***.

TABLE 2: Charges for $Fe(OH)_3(H_2O)_3$ Cluster from QC and QEq*

	$Fe(OH)_3(H_2O)_3$		
	QC[a]	QEq*[b]	α-Fe_2O_3 QEqX*
Fe	2.110	2.109	2.073
O	−1.169	−1.118	−1.382
H	0.466	0.415	

[a] Based on electrostatic potentials from HF/LAV3P***. [b] QEq but with the electronegativities modified as follows: $\chi_{Fe} = 3.500$, $\chi_O = 9.001$, and $\chi_H = 2.500$. The hardness and radius for Fe were also modified to $(1/2)J_{Fe} = 2.600$ and $R_{Fe} = 1.293$, respectively.

TABLE 3: Snap Bond Energies[a] (kcal/mol) for the $Fe(OH)_3(H_2O)_3$ Cluster from QC and MSX FF

	QC	MSX FF	UFF
$Fe-H_2O$	23.8	23.8	8.1
Fe−OH	134.5	134.5	63.4

[a] No change is allowed in the structure of the fragments.

TABLE 4: Geometries[a] for α-Fe_2O_3 Crystals from Experiment and from Force Fields

	exp[b]	MSX	UFF
Fe−O	1.946	1.900	1.852
Fe···O	2.116	2.099	2.135
Fe−O−Fe	119.7	123.4	91.6
O−Fe−O	102.5	102.8	80.5
a	13.7720	14.1338	22.523
b	5.0380	5.0526	3.712
c	5.0380	5.0527	3.845
α	120.0000	120.0009	124.839
β	90.0000	90.0044	93.854
γ	90.0000	89.9935	85.560

[a] Bond lengths are in angstroms, and bond angles are in degrees. [b] Reference 23.

As a test of the GVB model for Fe_2O_3, we used the MSX FF developed from the *ab initio* calculations on the $Fe(OH)_3(H_2O)_3$ cluster to predict the crystal structure of α-Fe_2O_3. The electrostatic charges were obtained using the QEq* parameters (with the QEqX program[19]). The crystal structure of α-Fe_2O_3 from the MSX FF (Table 4 and Figure 3) is in excellent agreement with experiment.[23] Thus the theoretical lattice parameters of $b = 5.0311$ Å, $c = 5.0319$ Å, $a = 13.760$ Å compare well with the experimental lattice parameters $b = c = 5.038$ Å, $a = 13.77$ Å.[23]

The GVB model of α-Fe_2O_3 suggests that the lowest energy surface is (001) since it does not require any CPI bonds to be broken. Indeed, experiment[24] shows that the preferentially exposed face is the (001) surface.

III.B. DTPs on Fe_2O_3 Clusters. To estimate the structure and energetics of the chemisorbed species, we first used *ab initio* QC calculations to optimize the structure of

$$Fe(OH)_2(H_2O)_2(DTP)$$

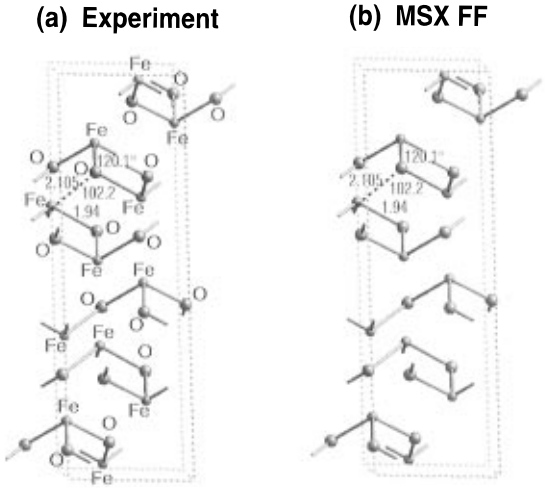

Figure 3. Geometric elements for the crystal structures of α-Fe_2O_3: (a) experiment[23] and (b) the MSX FF.

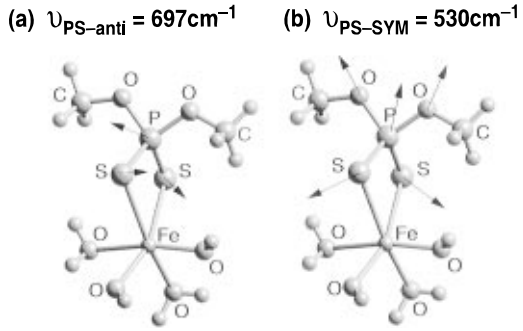

Figure 4. Vibrational modes of dimethyl DTP in the $Fe(OH)_2(H_2O)_2$-(DTP) cluster from QC calculations (HF/LAV3P***): (a) PS_{anti} and (b) PS_{sym}.

with R = Me. That is, we assume that DTP will displace one OH^- and one H_2O in bonding to the Fe surface. The results are shown in Figure 4, with key quantities tabulated in Table 5. These calculations lead to equivalent Fe−S bonds (2.63 Å versus 2.72 Å) with H_2O trans to the short bond and OH trans to the long bond. The snap bond energy[22] to remove the DTP is 164.5 kcal/mol.

We calculated vibrational frequencies of the $Fe(OH)_2(H_2O)_2$-(DTP) cluster with R = Me at the HF/LAV3P*** level, leading to the phosphorus−sulfur stretch modes in Figure 4.

Based on the *ab initio* results, we used the biased Hessian method to optimize the MSX FF to describe geometries, energies, and vibrations. Table 5 compares the *ab initio* and FF geometries. In the MSX FF, we describe the Fe−S interactions (off-diagonal nonbonded) using a Morse potential. The parameters were adjusted to reproduce the *ab initio* geometries of $Fe(OH)_2(H_2O)_2$(DTP) and the snap bond energy (164.5 kcal/mol) for DTP in the cluster.

Using the MSX FF, we calculated the vibrational frequencies (Table 6) for *R* = iPr, iBu, and Ph for the $Fe(OH)_2(H_2O)_2$(DTP) cluster. The predictions of the Fe-DTP modes and snap bond energies are shown in Table 7. The parameters of the new FF are listed in Table 6. For DTP we used parameters previously determined[7] for $Zn(DTP)_2$. The new parameters involving Fe are in Tables 8 and 9.

To obtain a measure of the relative binding energies, we calculated the energy change for the process in eq 10:

$$Zn(DTP)_2 + 2Fe(OH)_3(H_2O)_3 \xrightarrow{\Delta E} Zn(OH)_2(H_2O)_2 + 2Fe(OH)_2(H_2O)_2(DTP) \quad (10)$$

TABLE 5: Comparison of Geometries[a]-Calculated for the $Fe(OH)_2(H_2O)_2$(DTP) Clusters with R = Me

type	no.	QC[b]	MSX	UFF
DTP				
S−P	2	2.018	1.966	2.157
S−P−S	1	108.7	112.2	109.4
P−O	2	1.592	1.631	1.747
O−P−O	1	96.9	94.1	105.2
S−P−O	4	112.7	112.6	110.5
O−C	2	1.419	1.402	1.405
P−O−C	2	122.7	121.6	109.2
C−H	6	1.081	1.084	1.110
O−C−H	6	109.0	109.6	110.2
H−C−H	6	109.9	109.3	108.6
Fe−DTP				
Fe···S	1	2.626	2.638	2.495
Fe···S	1	2.715	2.682	2.596
Fe−OH				
Fe−O	2	1.883	1.937	1.912
Fe−O−H	2	121.4	125.2	99.7
O−Fe−O	1	106.6	112.3	86.9
Fe−H_2O				
Fe···O	2	2.236	2.264	2.094
H−O−H	2	109.1	107.1	102.1
O−H	6	0.947	0.949	0.995
Bond Energy (kcal/mol) $Fe(OH)_2(H_2O)_2$−DTP				
snap[c]		164.5	164.5	
adiadatic[d]		120.6	155.1	

[a] Bond lengths are in angstroms, and bond angles are in degrees. [b] HF/LAV3P***. [c] Fragment structure kept fixed as the bond is broken. [d] Fragment structure relaxed as the bond is broken.

TABLE 6: Averaged Vibrational Frequencies (cm^{-1}) and Vibrational Frequency Shifts Relative to Zn(DTP) for the P−S Stretch Modes of Various DTPs (Always the *tt* Conformation)

R		methyl	isobutyl	isopropyl	phenyl
PS_{anti}					
$Zn(DPT)_2$	MSX	647	647	654	650
	QC[a]	647[e]			
$Fe(OH)_2(H_2O)_2$(DTP)	MSX	656	656	662	660
	QC[a]	653[b,c]			
shift	MSX	9	9	8	10
	QC[a]	6			
PS_{sym}					
$Zn(DTP)_2$	MSX	553	547	542	583
	QC[a]	533[f]			
$Fe(OH)_2(H_2O)_2$(DTP)	MSX	548	545	536	573
	QC[a]	535[d]			
shift	MSX	−5	−2	−6	−10
	QC[a]	2			

[a] A scaling factor of 0.937 for PS_{anti} and 1.01 for PS_{sym} was applied to the QC frequencies. [b] Because of coupling with other vibrations, there are four unscaled modes at 652, 685, 713, and 742 cm^{-1}, all of which have significant P−S_{anti} character. We estimate that the unmixed PS_{anti} mode is at 697 cm^{-1}. Scaling by 0.937 leads to 653 cm^{-1}. [c] (I = 266.6 km/mol). [d] (I = 174.8 km/mol). [e] (I = 109.9 km/mol). [f] (I = 65 km/mol).

TABLE 7: Bond Energies[22] and Vibrational Frequencies for the Fe−DTP Modes[a] of Various DTPs from MSX

R		Me	iBu	iPr	Ph
bond energy (kcal/mol)	snap[b]	164.5	158.6	163.5	160.4
	adiabatic[c]	155.1	149.1	153.8	152.0
Fe−DTP vibn. freq. (cm^{-1})		412	409	414	407

[a] Unscaled. [b] Fragment structure fixed as bond is broken. [c] Fragment structure relaxed as bond is broken.

For R = Me we obtain $\Delta E_{(10)}$ = 50.1 kcal/mol from QC and 50.5 kcal/mol from MSX FF (see Table 10).

III.C. The α-Fe_2O_3 Surface. Cleaving α-Fe_2O_3 so that only DA bonds are broken leads to the (001) surface. Indeed, experiments[24] show that this is the low-energy surface of

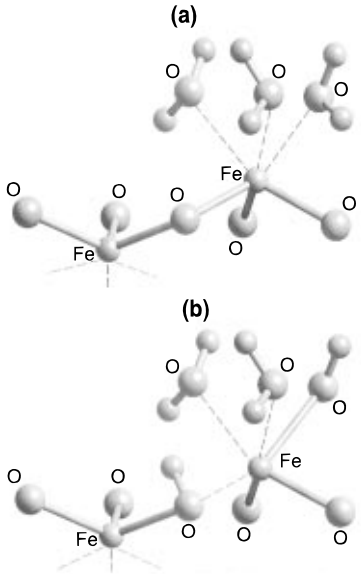

Figure 5. The GVB model of the α-Fe_2O_3 (001) surface used in the DTP binding calculations: (a) unreconstructed; (b) reconstructed by moving a proton from a surface H_2O to a bridging O. Only the surface atoms for a 1 × 1 unit cell are shown.

TABLE 8: Valence Parameters of the MSX FF for Fe Systems

bond (eq 3b)	K_R [(kcal/mol)/Å^2]	R_0 (Å)	D_R (kcal/mol)
Fe−O	468.9	1.933	134.5

angle (eq 4)	K_θ [(kcal/mol)/radian^2]	θ_0 (deg)	$K_{R\theta}$ (kcal/mol)/A·radian
Fe−O−H	103.4	129.0	
O−Fe−O	257.1	118.0	
Fe−O−Fe	150.0	147.0	−215

torsion (eq 5)	V_3 (kcal/mol)
X−Fe−O−X	0.4
X−Fe−S−X	0.0

TABLE 9: van der Waals Parameters of the MSX FF for Fe Systems

		type	R_v (Å)	D_v (kcal/mol)	ζ
diagonal[a]	Fe	exp-6[b]	4.540	0.055	12.00
off-diagonal	Fe···O	Morse[c]	2.400	5.00	16.00
	Fe···S	Morse[c]	2.770	14.6	12.00

[a] Diagonal parameters are from the Dreiding FF.[15a] [b] Equation 7. [c] Equation 8.

TABLE 10: Energy Change (kcal/mol) for the Process Defined in Eq 10

R	Me	iPr	iBu	Ph
MSX FF	50.5	31.5	33.3	29.4
QC (HF)	50.1			

α-Fe_2O_3, with no observed reconstruction. On the unreconstructed (001) surface of Fe_2O_3, this model would suggest that each Fe surface site has three H_2O molecules above the surface (forming DA bonds with Fe) and three O atoms below the surface (forming CPI bonds with Fe), as shown in Figure 5a. However, depending upon the environment, the actual surface likely has some H_2O and some OH^- at these sites. The ratio of OH^- to H_2O on the surface will be determined by the pH, by solvation effects, and by the surface reconstruction of Fe_2O_3. We use the simple surface reconstruction model in Figure 5b to account for such effects. This reconstructed surface has one solvent H_2O molecule replaced by an OH, leading to a CPI bond instead of a DA bond. To compensate, we assume that the proton is transferred to a subsurface O bonded to the same Fe (an CPI bond), transforming it to a DA bond. This structure (Figure 5b) balances the number of CPI and DA bonds on each Fe.

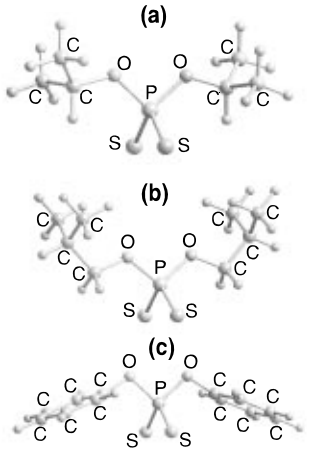

Figure 6. Structures for various DTP molecules: (a) R = iPr, (b) R = iBu, and (c) R = Ph. In each case we show the *tt* conformation. For a more detailed discussion on conformations and notation, see ref 7.

To describe the surface of α-Fe_2O_3 we carried out calculations with finite thickness slabs, separated by a vacuum. This allows proper two-dimensional periodic boundary condition calculations to be carried out with a program[17] written for full-dimensional periodic boundary conditions.[25] In the calculations the real part of the Ewald sums was carried out only over a single infinite slab, but the Fourier space terms include interactions between slabs. If the slabs are too close, then they interact with each other through the real part sum of the Ewald energy. On the other hand, too large a separation between the slabs leads to slow convergence of the Fourier reciprocal lattice sums. Consequently we considered the reconstructed surface with a monolayer of DTP on the surface and varied the separation between the slabs. We found that a slab separation of 15−45 Å is best and usually used 25 Å for subsequent calculations.

IV. The DTP Film on α-Fe_2O_3

IV.A. Calculations. We studied the structures and energies of DTP for R = iPr, iBu, and Ph (see Figure 6) bound to the reconstructed surfaces. In each case we considered the various conformations of the R groups (*tt*, *tg*, *gg*), the various possible binding patterns (S binds wholly to one Fe site or bridges over multiple Fe sites), and the various possible unit cells to achieve the most stable monolayer. Figures 7−9 show the optimum packing pattern for the three DTP species on the surface. From the calculations we find the following:

(i) The most stable monolayers for isobutyl, isopropyl, and phenyl DTP molecules each lead to one DTP for each pair of surface Fe. The result is a monolayer with a 2 × 1 unit cell. This is referred to as 1/2 coverage.

(ii) Each S atom of a DTP molecule bridges between two Fe sites.

(iii) The monolayer prefers the g^-g^- conformation for R = iPr and Ph and the tg^- conformation for R = iBu.

Results for optimum packing are tabulated in Table 11.

IV.B. Comparison with Wear Performance. It is generally agreed that the primary function of ZnDTP is to form wear resistant films on rubbing surfaces. However, the nature of the films formed from ZnDTP has long been a matter of debate. Generally, surface films may be formed by physical adsorption, chemisorption, and chemical reaction as temperature increased. On the basis of experimental observations,[6,26,27] adsorption is the initial step in antiwear film formation. It has been

TABLE 11: Packing of Various DTP Molecules on the (001) Reconstructed Surface of α-Fe_2O_3; In Each Case the Unit Cell Is 1 × 2 Unit

R	DTP conformation (O−P−O−C in deg)	Fe···S[a] x_1,x_2,y_1,y_2 (Å)	$\Delta E^b_{(11b)}$ (kcal/mol)	maximum cam lobe wear[c] (in.)
Me[d]	−63/−67 (g^-g^-)	2.75, 2.82, 2.82, 2.86	253.5	
iPr	−69/−74 (g^-g^-)	2.73, 2.81, 2.80, 2.88	254.7	0.0025 ± 0.0009
iBu	−173/−77 (tg^-)	2.75, 2.84, 2.78, 2.91	242.6	0.0081 ± 0.001
Ph	−64/−75 (g^-g^-)	2.93, 2.98, 2.65, 2.83	240.8	0.0123 ± 0.0039

[a] See Figures 7−9. [b] The cohesive energies from eq 11b. [c] See ref 6a. We consider results for alkyl secondary in this reference comparable to iPr; alkyl primary comparable to iBu; aryl comparable to Ph. [d] Dimethyl DTP has not been tested in this engine test because of poor oil solubility.

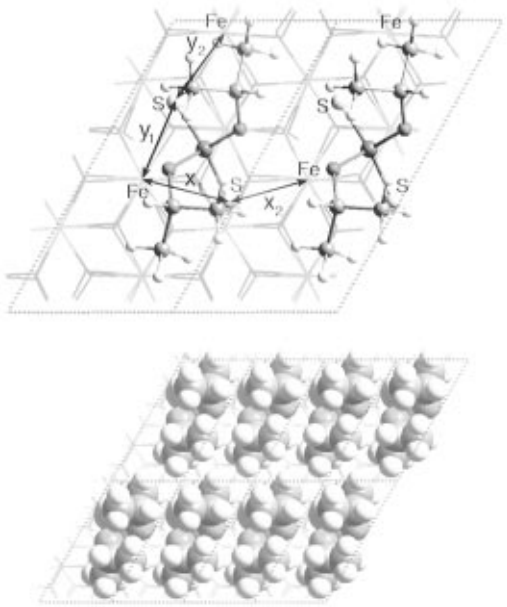

Figure 7. Packing pattern of isopropyl DTP molecules in 1 × 2 unit cells of the reconstructed (001) surface of α-Fe_2O_3. The conformation is g^-g^-. (a, top) Ball and stick model with two 1 × 2 unit cells. (b, bottom) CPK model with eight 1 × 2 unit cells. (See Table 11 for x_1, x_2, y_1, y_2 values.)

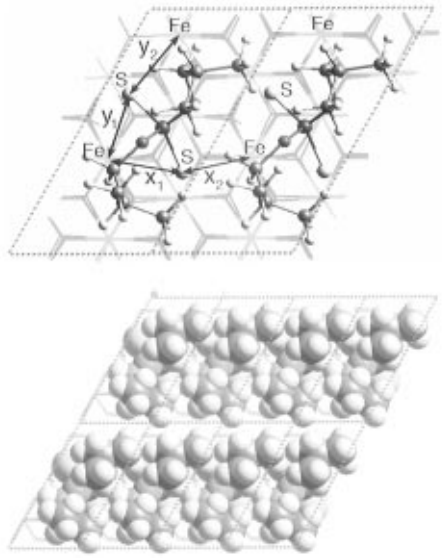

Figure 8. Same as Figure 7 but for R = isobutyl. The conformation is tg^-.

proposed[26] that the ZnDTP initially physisorbs on the surface and subsequently reacts with hydroxyl groups on the metal surface to form a chemisorbed Zn-depleted DTP layer. This is supported by experiments using ^{65}Zn- and ^{14}C-labeled ZnDTP solutions,[26] which show the presence of a chemisorbed layer containing no zinc. As the temperature is increased further, the films convert to inorganic, amorphous phosphates (with some S) having a range of chain lengths.[28]

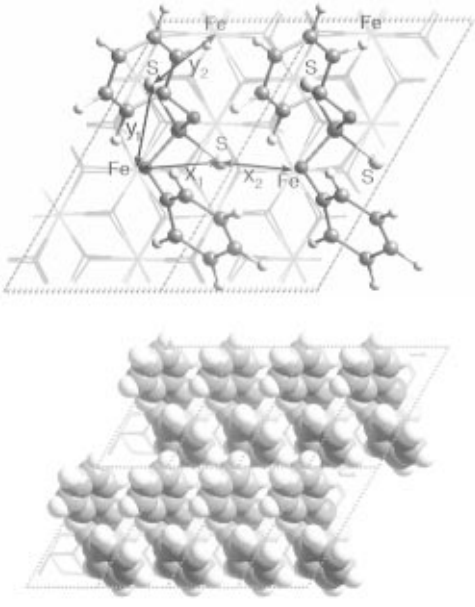

Figure 9. Same as Figure 7, but for R = phenyl. The conformation is g^-g^-.

Some progress has been made in the experimental characterization of how wear inhibitors interact with metal oxide surfaces to provide wear protection.[5] For example, inelastic electron tunneling spectroscopy (IETS) showed that the bond strength of DTP to Al_2O_3 surfaces (as measured by shifts in P−S vibrational frequencies) does correlate with antiwear performance of these zinc salts[29] in internal combustion (cast iron) engines. Iron and iron oxides surfaces would be more relevant in lubrication applications than Al_2O_3, but similar IETS studies on iron have not yet been successful.

As a first step in trying to elucidate the mechanism of wear performance, we considered that the DTP is dissociated from the Zn to form a chemisorbed monolayer as described in section IV.A. To provide some measure for comparing the various DTP binding to the surface, we calculated the relative binding energies for the process in (11a):

$$\mathrm{Zn(DTP)_2} + 2\alpha\text{-}\mathrm{Fe_2O_3(OH)(H_2O)} \xrightarrow{\Delta E} \mathrm{Zn(OH)_2(H_2O)_2} + 2\alpha\text{-}\mathrm{Fe_2O_3(DTP)} \quad (11a)$$

and the total cohesive energy for binding of DTP to the α-Fe_2O_3 surface (with OH and H_2O removed)

$$E_{CO4} = E(\alpha\text{-}\mathrm{Fe_2O_3(DTP)}) - E(\mathrm{DTP}) - E(\alpha\text{-}\mathrm{Fe_2O_3}) \quad (11b)$$

As shown in Table 11, the cohesive energy (11b) for the best packing are in the order

isopropyl (255 kcal/mol) > isobutyl (243 kcal/mol) > phenyl (241 kcal/mol)

Indeed, full engine tests lead to observed camshaft antiwear performance (maximum wear) for these types of ZnDTP salts[6a]

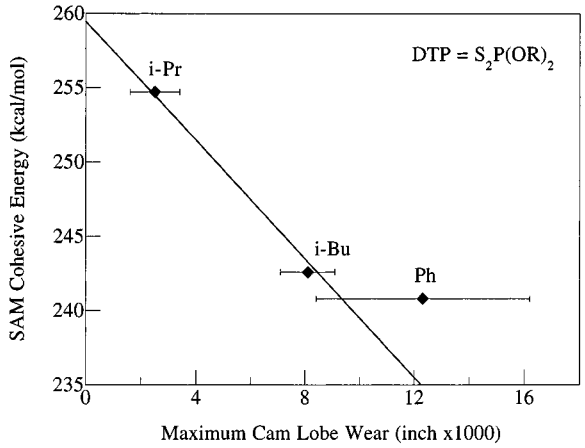

Figure 10. Correlation of SAM cohesive energy with camshaft wear.

TABLE 12: Vibrational Frequencies (cm^{-1}) for iPr, iBu, and Ph on the α-Fe_2O_3 surface[a]

PS_{anti}			PS_{sym}		
iPr	iBu	Ph	iPr	iBu	Ph
Full Monolayer Coverage (1 × 2 Cell)					
690(*gg*)	676(*tg*)	751(*gg*)	551(*gg*)	553(*tg*)	657(*gg*)
Low Coverage[b]					
682(av)	656(av)	731(av)	539(av)	555(av)	620(av)
654(*tt*)	647(*tt*)	650(*tt*)	542(*tt*)	547(*tt*)	583(*tt*)
668(*tg*)	662(*tg*)	731(*tg*)	542(*tg*)	552(*tg*)	620(*tg*)
682(*gg*)	669(*gg*)	743(*gg*)	539(*gg*)	571(*gg*)	646(*gg*)

[a] The corresponding conformations (*gg*, *tg*, *tt*) are in parentheses. The average conformation (av) is based on the Boltzmann distribution (at 300 K) calculated from the relative energetics among *tt*, *tg*, and *gg* given in Table 13. [b] Based on the 4 × 2 unit cell.

TABLE 13: Relative Energies (kcal/mol) of the DTP Conformation with One Molecule per (2 × 4) Unit Cell

	iPr	iBu	Ph
tt	0.0	0.0	0.0
tg	3.0	0.8	−4.5
gg	−4.9	0.3	0.7

that follow the same trend:

secondary alkyl (0.002 in.) < primary alkyl (0.008 in.) < aryl (0.012 in.)

This relation is shown graphically in Figure 10. This suggests that there is a strong correlation between the cohesive energy of the SAM film and the antiwear performance.

This is the first correlation found between a physical property (from modeling) and the antiwear performance measured by actual engine tests. Based on this correspondence, candidates for new wear inhibitors are being compared and prioritized (by calculating the structures and determining the cohesive energy of the SAM film) before synthesis and testing.[8]

IV.C. Vibrational Spectra. In order to provide for additional tests of the SAM model and of the theoretical predictions, we calculated vibrational frequencies of the DTP/SAM films and for the various DTPs on an α-Fe_2O_3 surface at low concentration. The vibrational frequencies of a DTP on the surface at low concentration were obtained using a 2 × 4 unit cell and weighting the vibrational frequencies for the various conformations using a Boltzmann factor based on the relative binding energies of the conformations. The results are given in Tables 12 and 13.

V. Summary

We studied the geometries, energetics, and vibrations of DTP molecules on Fe clusters and on α-Fe_2O_3 surfaces using *ab initio* quantum chemistry and molecular mechanics methods. The MSX FF [based on the GVB model of Fe_2O_3 and developed from *ab initio* QC calculation studies on the $Fe(OH)_3(H_2O)_3$ cluster] predicts correctly the α-Fe_2O_3 crystal structure.

We considered DTP = $(RO)_2PS_2$ with R = methyl (Me), isobutyl (iBu), isopropyl (iPr), and phenyl (Ph). These results show that DTP molecules bind very strongly on the Fe_2O_3 surface. No significant differences in binding energies were found for primary (Me, iBu) and secondary (iPr) alkyl DTPs on isolated Fe clusters.

For a given conformation we found little shift in the frequency upon binding in the cluster models. However, we find that the vibrational frequencies of the PS modes for DTPs bound to Fe sites on a model surface are sensitive to the conformation of the OR groups (*tt*, *tg*, *gg*). Therefore, the shift in PS vibrational frequency for DTPs bound to the surface are largely due to the change in conformational preferences due to packing energies.

We developed a surface reconstruction model of the α-Fe_2O_3 (001) surface to include surface OH likely in normal engine environments. We find that isobutyl, isopropyl, and phenyl DTP molecules each lead to a self-assembled monolayer (SAM) with 1/2 coverage.

VI. Conclusion

We find that the relative binding energies of forming a SAM on Fe_2O_3 correlates with the antiwear performance observed in actual engine tests. This suggests that the structures and energies of the SAM be used to predict the performance of wear inhibitors prior to synthesis and experiment. This correlation is now being used to help develop new wear inhibitors.[8]

Acknowledgment. This research was supported by the Chevron Chemical Company (Oronite Technology group), and we thank Bob Lewis for his encouragement. It was also supported by grants from the DOE-BCTR and NSF (CHE 95-22179 and ASC 92-100368). The facilities of the MSC are also supported by grants from Chevron Petroleum Technology Co., Asahi Chemical, Aramco, Owens-Corning, Exxon, Asahi Glass, Nippon Steel, Chevron Research Technology Co., Hercules, Avery Dennison, BP Chemical, and Beckman Institute. Part of the calculations were carried out at the National Center for Supercomputer Applications (U. Illinois) and the JPL Supercomputer Center.

References and Notes

(1) Yamaguchi, E. S.; Primer, R. L.; Aragón, S. A.; Labrador, E. Q. *Tribol. Trans*., in press.

(2) Yamaguchi, E. S.; Ryason, P. R. *Proceedings of the Fourth International Symposium on the Performance Evaluation of Automotive Fuels and Lubricants*; CEC: Birmingham, U.K., 1993; p 1.

(3) Wooton, D. L.; Hughes, D. W. *Lubr. Eng.* **1987**, *43*, 736. Willermet, P. A.; Pieprzak, J. M.; Dailey, D. P.; Carter, R. O., III; Lindsay, N. E.; Haack, L. P.; deVries, J. E. *J. Tribol.* **1991**, *113*, 738. Johnston, G.; Cann, P. M.; Spikes, H. A. *Leeds-Lyon Symposium on Tribology*; Butterworths: London, 1986; pp 128−134. Lansdown, A. R. In *Chemistry and Technology of Lubricants*; Mortier, R. M., Orszulik, S. T., Eds.; Blackie: Glasgow and London, 1995.

(4) Roby, S. H.; Supp, J. A. SAE 952342; SAE: Warrendale, PA, 1995. Korcek, S. *Tribology 2000: 8th Intl. Coll.*; Bartz, W. J., Ed.; Technische Akademic Esslingen: Octfildem, 1992; pp 11.1-1−11.1-6. Williamson, W. B.; Perry, J.; Goss, R. L.; Gandhi, H. G.; Barson, R. E. SAE 841406; SAE: Warrendale, PA, 1984. Hayashi, S.; Stonebraker, P. M.; Cisson, C. M.; Rausina, G. A. *Toraiborojisuto* **1995**, *40*, 286.

(5) Standardized Test Price Update and Historical Summary, Engine Lubricants Research Department (Southwest Research Institute, Houston, 1995−1996).

(6) (a) McGeehan, J. A.; Graham, J. P.; Yamaguchi, E. S. SAE 902162; SAE: Warrendale, PA, 1990. (b) Roby, S. H. *Lubr. Eng.* **1991**, *47*, 413. (c) Benchaita, M. T. *Lubr. Eng.* **1991**, *47*, 893.

(7) Jiang, S.; Dasgupta, S.; Blanco, M.; Frazier, R.; Yamaguchi, E. S.; Tang, Y.; Goddard, W. A., III *J. Phys. Chem.* **1996**, *100*, 15760.

(8) Jiang, S.; Frazier, R.; Yamaguchi, E. S.; Ho, A.; Goddard, W. A., III. Private communication.

(9) Ramachandran, S.; Tsai, B.-L.; Blanco, M.; Chen, H.; Tang, Y.; Goddard, W. A., III. *J. Phys. Chem.* **1997**, *101*, 83. Ramachandran, S.; Tsai, B.-L.; Blanco, M.; Chen, H.; Tang, Y.; Goddard, W. A., III. *Langmuir* **1996**, *12*, 6419. Ramachandran, S.; Tsai, B.-L.; Blanco, M.; Chen, H.; Tang, Y.; Goddard, W. A., III. In *New Techniques for Characterizing Corrosion and Stress Corrosion*; Jones, R. H., Baer, D. R., Ed.; The Minerals, Metals & Materials Society; 1996; p 117.

(10) Greeley, B. H.; Russo, T. V.; Mainz, D. T.; Friesner, R. A.; Langlois, J.-M.; Goddard, W. A., III; Donnelly, R. E.; Ringnalda, M. N. *J. Chem. Phys.* **1994**, *101*, 4028.

(11) Ringnalda, M. N.; Langlois, J.-M.; Greeley, B. H.; Murphy, R. B.; Russo, T. V.; Cortis, C.; Muller, R. P.; Marten, B.; Donnelly, R. E., Jr.; Mainz, D. T.; Wright, J. R.; Pollard, W. T.; Cao, Y.; Won, Y.; Miller, G. H.; Goddard, W. A., III; Friesner, R. A. *PS-GVB v2.24*; Schrödinger, Inc.: Portland, OR, 1995.

(12) Hay, P. J.; Wadt, W. R. *J. Chem. Phys.* **1985**, *82*, 270; **1985**, *82*, 284; **1985**, *82*, 299.

(13) Frisch, M. J.; Pople, J. A.; Binkley, J. S. *J. Chem. Phys.* **1984**, *80*, 3265.

(14) Chirlian, L. E.; Francl, M. M. *J. Comput. Chem.* **1987**, *8*, 894. Woods, R. J.; Khalil, M.; Pell, W.; Moffat, S. H.; Smith, V. H., Jr. *J. Comput. Chem.* **1990**, *11*, 297. Breneman, C. M.; Wiberg, K. B. *J. Comput. Chem.* **1990**, *11*, 361.

(15) (a) Mayo, S. L.; Olafson, B. D.; Goddard, W. A., III. *J. Phys. Chem.* **1990**, *94*, 8897. (b) Rappé, A. K.; Casewit, C. J.; Colwell, K. S.; Goddard, W. A., III; Skiff, W. M. *J. Am. Chem. Soc.* **1992**, *14*, 10025.

(16) Dasgupta, S.; Goddard, W. A., III. *J. Chem. Phys.* **1989**, *90*, 7207. Dasgupta, S.; Yamasaki, T.; Goddard, W. A., III. *J. Chem. Phys.* **1996**, *104*, 2898.

(17) *BIOGRAF/POLYGRAF*, V 3.21 (Caltech Version V 3.30); Molecular Simulations Inc.: San Diego, CA.

(18) Rappé, A. K.; Goddard, W. A., III. *J. Phys. Chem.* **1991**, *95*, 3358.

(19) The extension of QEq to infinite systems (periodic boundary conditions) was developed (QEqX) by N. Karasawa, G. H. Miller, and W. A. Goddard III, to be published.

(20) Scully, J. C. In *The Fundamentals of Corrosion*, 3rd ed.; Pergamon Press: Oxford, 1990.

(21) Jiang, S.; Frazier, R.; Yamaguchi, E. S.; Goddard, W. A., III. Manuscript in preparation.

(22) The snap bond energy for A−B is obtained by fixing the internal coordinates of A and of B and then separating the fragments to infinity.

(23) Wyckoff, R. W. G. *Crystal Structures*; Interscience: New York, NY, 1963.

(24) Eggleston, C. M.; Hochella, M. F., Jr. *Am. Mineral.* **1992**, *77*, 911.

(25) Karasawa, N.; Goddard, W. A., III. *J. Phys. Chem.* **1989**, *93*, 7320. Karasawa, N.; Dasgupta, S.; Goddard, W. A., III. *J. Phys. Chem.* **1991**, *95*, 2260.

(26) Dacre, B.; Bovington, C. B. *ASLE Trans.* **1983**, *25*, 546; **1983**, *26*, 33.

(27) Plaza, S. *ASLE Trans.* **1987**, *30*, 233.

(28) Willermet, P. A.; Dailey, D. P.; Carter, R. O., III; Schmitz, P. J.; Zhu, W. *Tribol. Int.* **1995**, *28*, 177. Willermet, P. A.; Pieprzak, J. M.; Dailey, D. P.; Carter, R. O., III; Lindsay, N. E.; Haack, L. P.; deVries, J. E. *ASME J.O.T.* **1991**, *113*. Willermet, P. A.; Carter, R. O., III; Boulos, E. N. *Tribol. Int.* **1992**, *25*, 371. Bell, J. C.; Delargy, K. M.; Seeney, A. M. *Proceedings of the 18th Leeds-Lyon Symposium on Tribology*; Elsevier: Amsterdam, 1992. Bell, J. C.; Delargy, K. M. *6th Intl. Congress on Tribology*; Budapest, Hungary, 1993. Willermet, P. A.; Dailey, D. P.; Carter, R. O., III; Schmitz, P. J.; Zhu, W.; Bell, J. C.; Park, D. *Tribol. Int.* **1995**, *28*, 165. Yin, Z.; Kasrai, M.; Bancroft, G. M.; Laycock, K. F.; Tan, K. H. *Tribol. Int.* **1993**, *26*, 333.

(29) Yamaguchi, E. S.; Ryason, P. R. *Tribol. Trans.* **1993**, *38*, 243.